Journal of Nuclear Materials 379 (2008) 124–132

Contents lists available at ScienceDirect

Journal of Nuclear Materials

journal homepage: www.elsevier.com/locate/jnucmat

Corrosion behaviour of reinforced concrete: Laboratory experiments and archaeological analogues for long-term predictive modelling

V. L'Hostis [a,*], F. Foct [b], P. Dillmann [c,d]

[a] CEA, DEN, DPC, SCCME, Laboratoire d'Etude du Comportement des Bétons et des Argiles, F-91191 Gif-sur-Yvette, France
[b] EDF R&D/MMC, Site des Renardières, 77818 Moret-sur-Loing cedex, France
[c] CEA/CNRS Laboratoire Pierre Süe, 91191 Gif-sur-Yvette cedex, France
[d] CNRS IRAMAT, UMR 5060, France

A B S T R A C T

In the context of the nuclear waste storage, reinforced concrete will be used for various purposes such as cell structures and some types of containers (e.g. for intermediate level wastes). These structures are required to be safe and reliable in varying environments for long periods of time (up to several hundred years). This paper presents a specific approach that is developed in France at CEA and EDF for the prediction of long-term behaviour of such structures. It discusses the experimental and theoretical approaches which have been developed. It is based on interactive studies dedicated to short term experimentations (corrosion and mechanical behaviour of structures), characterization and specific tests on archaeological analogues, both used to develop mechanistic understanding and modelling of corrosion and mechanical behaviour of reinforced concrete. Advantages and limits of these different and complementary aspects are presented and discussed. Moreover the prediction results of a specific mechanistic model have been confronted to real structures exposed to atmospheric conditions for many years.

1. Introduction

Corrosion of rebars in reinforced concrete structures is the primary cause of structural deterioration of bridge decks, tall buildings, tunnels and reinforced containers. Generally, this composite material is able of withstanding a wide range of environments for a certain period of time. As concrete is porous and both moisture and oxygen can move through the pores and micro-cracks in concrete, the basic requirements for the onset of active corrosion of mild or high strength ferritic reinforcing steels are present. Active corrosion does not occur quickly in most cases because the pore fluid contains high levels of calcium, sodium and potassium hydroxide, which maintain a pH between 12 and 13. At this range of alkalinity the steel remain passive [1], forming a passive corrosion layer that is self maintaining and prevents active corrosion.

Usually, the deterioration process associated has the following three stages [2]:

- *Initiation*. During this long time the corrosion rate is very low despite the ingress of the two main aggressive reagents for the steel ie chlorides or the carbonation front, from the environment to the steel.
- *Depassivation*. This step happens when the conditions required for the onset of corrosion are fulfilled thanks to the chloride, or the carbonation conditions of concrete at the steel/concrete interface.
- *Propagation*. The reinforcement corrosion causes significant growth of expansive corrosion products. Then, internal micro cracking and spalling of the concrete cover appear. They are due to the high tensile stresses generated by the expansive volume of the corrosion products [3,4].

In the context of the nuclear waste storage, reinforced concrete will be used for various purposes such as cell structures and some types of containers (e.g. for intermediate level wastes). These structures are required to be safe and reliable in challenging and varying environments for periods of time that can potentially range up to several hundred years. Due to these long-term applications, specific studies have to be developed:

- It is necessary to complete classical laboratory short term experiments by studies of system formed on the very long-term (archaeological analogues).
- Phenomenological modelling has to be developed and validated, instead of empirical models that can be found in the literature. To achieve input data and validate these models, archaeological analogues and laboratory studies must be continuously confronted.

* Corresponding author. Tel.: +33 169 08 32 13; fax: +33 169 08 84 41.
E-mail address: valerie.lhostis@cea.fr (V. L'Hostis).

0022-3115/$ - see front matter © 2008 Elsevier B.V. All rights reserved.
doi:10.1016/j.jnucmat.2008.06.018

- The passive corrosion state has to be considered. As a matter of fact, one has to ask if the passive corrosion rates happening during a very long time could lead to the formation of an oxide layer able to generate mechanical stresses in the concrete cover.

In this context, two programs are conducted in collaboration in France by the French *Commissariat à l'Energie Atomique* (CEA) (*CIMETAL* research program) and by *Electricité de France* (EDF) (*Stockage* research program). These studies have enabled the identification of the parameters that have to be taken into account for a phenomenological modelling of corrosion in concrete. These parameters, as well as the organization of the approach are presented in Fig. 1 and will be detailed in the present paper.

Carbonation or chloride ingress within the concrete fixes the chemical conditions of the interstitial solution at the concrete/steel interface. At the same time, oxygen transport in the concrete cover imposed the redox potential of this solution. For some chemical and redox conditions at the steel/concrete interface, depassivation of the rebar occurs. Then, during the active corrosion process, the corrosion rate depends on several parameters: water saturation level of the concrete, as well as the corrosion products layer, charge transfer resistance in case of a thin oxide layer, and the oxygen transport within the corrosion products layer. Corrosion of steel leads to the formation of iron II or III ions, depending on the chemical and the redox conditions within the interstitial solution of the concrete. Ferrous species formed during the corrosion process may diffuse or precipitate in concrete. Depending on the part of oxide which precipitates at the metal/concrete interface, the oxide layer may induce tensile stress/strain field in the surrounding concrete.

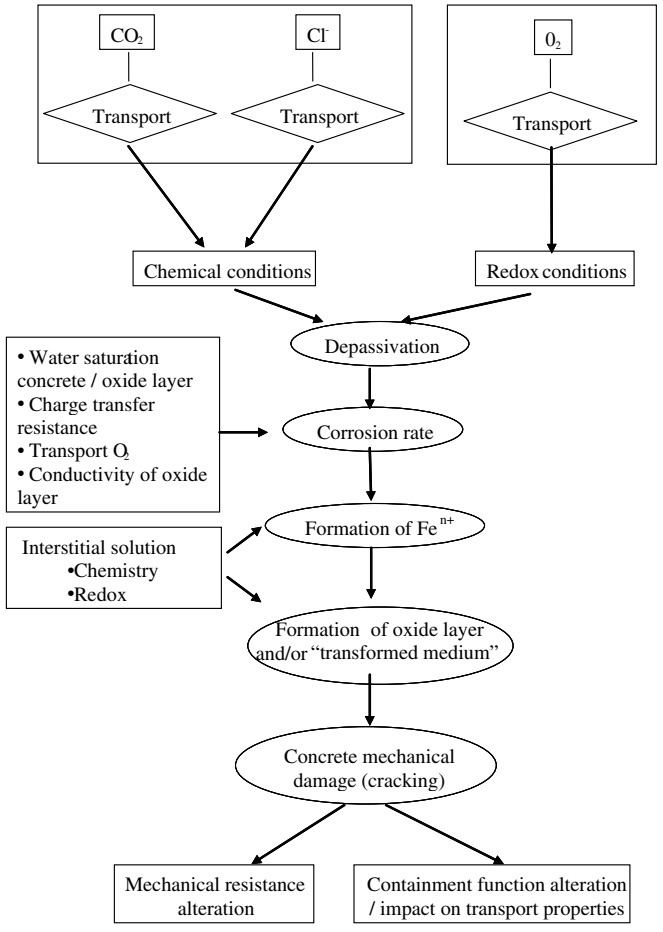

Fig. 1. Organisation of a mechanistic approach for corrosion of steel in concrete.

This would lead to concrete cracking. This degradation mechanism affects the mechanical and containment properties of these structures and therefore has to be assessed.

2. Conditions for passive/active corrosion state

The first step of the approach is to identify the conditions for passive or active corrosion states. These conditions can be fixed by the chemical conditions (chlorinated or carbonated concrete) but also by the physico-chemical conditions (oxygen availability, concrete water saturation degree).

2.1. Water saturated chlorinated environments

When chloride is present in the concrete pore water, pitting is a possibility and it is characterized by well documented pitting initiation potentials and by a 'protection potential' Eprot. The mechanisms of localised corrosion indicate that propagation of pitting (and also of crevice corrosion) is possible only above the 'protection potential' and is not possible below that potential. These mechanisms and the value of this protection potential were determined and confirmed by a series of experimental studies [5]. Typical values of Eprot for C-steel in chloride are about −0.55 to −0.60 Vsce, at room temperature. This is important for the storage of nuclear waste since oxygen is expected to be consumed in the course of time, and the potential is expected to decrease below Eprot.

To resume, in an aerated alkaline concrete which is not contaminated by chloride, C-steel is passive. However, when oxygen is consumed and when anoxic conditions are reached, the risk of pitting initiation disappears. Moreover, even if pitting has started during the aerated period, the propagation of existing pits is stopped.

Passive systems are thus quite safe and are preferable to systems where general corrosion is possible. In addition the generation of hydrogen under anoxic conditions is considerably less for passive systems than for systems that corrode in a general manner.

2.2. Atmospheric carbonated environments

In order to assess depassivation conditions in carbonated environments, steel coupons have been immersed in five different electrolytes, with pH ranging from 13 to 8.3. These aqueous solutions were chosen to simulate the interstitial concrete pore water at various degrees of carbonation. Electrochemical techniques (polarization curves, free corrosion potential measurements) and surface analyses (EDS, XRD, XPS) were carried out to assess the corrosion behaviour of the steel samples [6,7]. The results indicate that the transition pH is between 10 and 9.4. XPS results indicate a passivation of mild steel for pH values ranging from 13 to 10 due to the formation of a thin iron III oxide layer. Immersion tests highlight the importance of the buffering effect of the carbonate content. At the free corrosion potential in an aerated solution, a decrease of the carbonate content increases the corrosion rate. On the opposite, at low electrode potential, the kinetics of oxidation increases with the carbonate content. Main conclusions of this study are that to understand the transition from passive to active behaviour of mild steel pH should not be considered in a first approach but as a priority the electrode potential and carbonate content buffering.

3. Formation of iron oxides

In order to be able to mechanistically model the long-term corrosion behaviour of reinforcements, two main aspects has to be assessed: the corrosion pattern (structure, nature and dissolution of iron oxides) and the corrosion rates (metal loss and expansion coefficient of the oxide layer).

3.1. Experimental characterization of the corrosion pattern

3.1.1. Water saturated chlorinated media

Steel pills have been embedded in cement paste containing 5 g/L or 10 g/L free chlorides in their interstitial solution. Steel placed under these conditions presents thick corrosion layers (until 200 μm) after 700 days exposition in alkaline chlorinated solution. Corrosion pattern also shows localised corrosion zones (pits depth maximum 200 μm). Moreover, corrosion products layer that have been identified locally with microspectroscopy Raman are hydrated iron hydroxides. In the corrosion products layer, mainly goethite (α-FeOOH) and lepidocrocite (γ-FeOOH) have been identified (Fig. 2(A)).

Then average concentration profiles have been realized for iron oxygen, calcium and silica, from the metal/CPL interface to the cement paste. All samples placed in presence of chloride have the same profiles (Fig. 2(B)):

- metal containing localized corroded zones (pits),
- corrosion products layer number 1 containing iron, oxygen and around 5% in weight of calcium, with a constant concentration in this layer,
- corrosion products layer number 2 containing iron, oxygen and calcium with an increasing concentration until wt. 10% ,
- transformed medium, defined by the presence of iron, oxygen, calcium and silicium. In this layer, iron content decreases whereas calcium and silica contents are increasing,
- cement paste which does not contains any corrosion products, where iron, calcium and silica contents are constant.

3.1.2. Atmospheric carbonated media

The general pattern encountered on archaeological corroded metallic reinforcements in reinforced concrete structures exposed to the atmosphere (50–650 years) is also made up of a multilayer structure [19]. This pattern can be illustrated by observations made on the Saint Gervais Church, in Paris, aged of 250 years (Fig. 3) [19]. The corrosion layout can be described as the metallic substrate (M), the corrosion product layer (CPL), the Transformed Medium (TM) and the Binder (B). An analogy can be seen with the corrosion pattern obtained even at short term (2 years) in water saturated chlorinated environments (previous section).

For all samples, the CPL is constituted of a matrix of iron oxi-hydroxides (mainly goethite α-FeOOH) containing marblings of iron oxides (magnetite Fe_3O_4 and/or maghemite γ-Fe_2O_3). The TM is composed of minerals coming from the CPL (iron oxi-hydroxides) and from the binder (calcite and quartz in this case).

3.2. Modelling the formation of corrosion products layer and transformed medium

The expansion caused during the CPL formation is known to be responsible for the corrosion-related deteriorations in concrete. On the other hand, the second layer containing corrosion products, the transformed medium, is not expected to cause any further damage, since it only consists of ferrous ions diffused and precipitated into the concrete microstructure.

The formation of this transformed medium might happen in two possible ways:

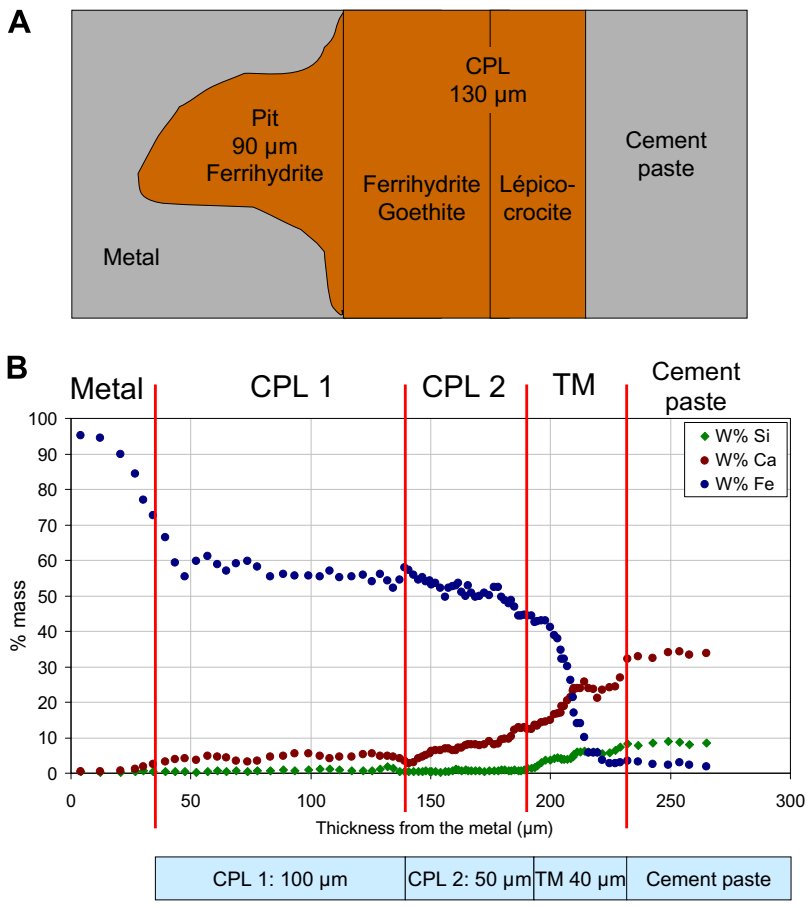

Fig. 2. (A) Schematic representation of the corrosion pattern; (B) average concentration profiles for iron, calcium and silicium from the metal to the sane cement paste. Samples of steel embedded in concrete containing 5 g/L free chlorides in interstitial solution.

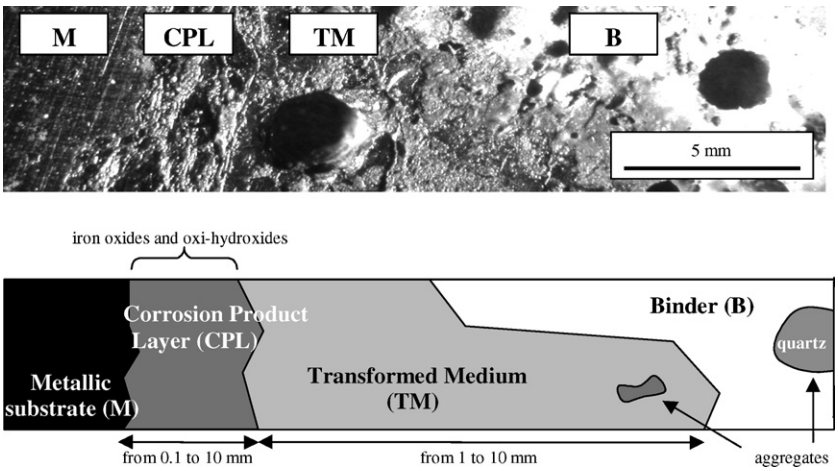

Fig. 3. Macro photograph of a cross-section of Saint Gervais Church sample and schematic section of the corrosion system (M: metal; CPL: corrosion product layer, TM: transformed medium; B: binder) [19].

- *Possibility 1*: Some ferrous ions formed at the metal interface might be transported through the corrosion product layer and later precipitate in the concrete.
- *Possibility 2*: The 'transformed medium' might be formed due to the dissolution of the corrosion products layer into ferrous ions and re-precipitation of these ions further in the concrete.

In order to develop a reliable model, the verification of these two hypotheses is crucial. Indeed, in the 1st case, only a fraction of the ferrous ions formed in the corrosion process will be directly present in CPL and therefore cause damage. If we imagine there is no dissolution, the accumulation of CPL, even if decreased by the fraction of ferrous ions diffusing in the concrete (TM), may lead to cracking after a long period. In the 2nd case two scenarii are possible. On the one hand, all of the formed ferrous ions can cause damage (as CPL), if the iron oxide dissolution and progress in concrete (forming the TM) occurs later on, on the other hand, the damage could be limited or avoided if iron diffusion to TM and corrosion rate occur at the same time with similar kinetics.

In order to assess these hypotheses, chemical-transport codes (Chess and Hytec) have been used [8]. Results showed that the iron speciation is strongly influenced by the concrete interstitial solution. In particular the influence of potential on the nature of iron oxides was highlighted. Under low redox conditions the chelating of Fe^{2+} by SO_4^{2-} and HCO_3^- increases the solubility of iron oxides and modify their nature (formation of siderite, $FeCO_3$).

The iron oxides dissolution was then simulated with a numerical reactive transport model (Hytec) assuming local equilibrium. Results indicated that the dissolution of goethite is negligible due to its very low solubility. On the contrary, siderite dissolution is low as well but not negligible. These results were also observed in precedent studies [9] for mild steel buried in clayed soils. The oxygen flux controls the dissolution of siderite due to the local oxidation of $FeCO_3^0$ into ferric oxy-hydroxides. This mechanism entails a local chemical and microstructural change of the carbonated concrete.

Fig. 4 presents chemical-transport calculations results that showed that under stationary conditions, the dissolved thickness of siderite is around 0.3 μm/year. However, during a humid season (6 months) stationary conditions are barely reached. Actually, the dissolved thickness is strongly dependent on initial conditions. Curves on Fig. 4 present two extreme conditions depending on the presence or absence of oxygen in the water saturated concrete. The effective concentration of oxygen depends on the chemistry

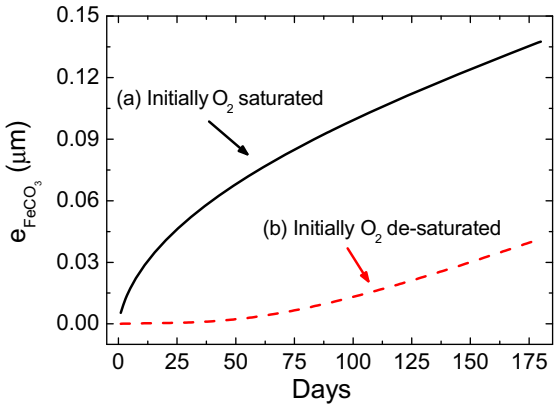

Fig. 4. Increase of equivalent layer thickness of dissolved siderite evaluated from ferrous flow in the carbonated concrete matrix, (a) interstitial solution is initially saturated with oxygen (250 μmol/L), (b) interstitial solution is initially de-saturated with oxygen (0 μmol/L).

of the resaturation water and on the kinetic of resaturation. This estimated kinetics for the dissolution of CPL showed that the formation of the transformed medium has to be taken into account while considering which part of iron oxides takes part in the mechanical damage of the concrete cover.

4. Corrosion rates

4.1. Passive corrosion state

Usually, the corrosion modelling of mild steel under passive conditions is based on the physical description of the growing of a dense corrosion layer. In this particular case, the corrosion rate and the growth of the oxides layer is limited by species motion in the solid phase: electron or point defect motion (anionic or cationic) [10,11]. Thus, these conditions lead to a very low value of the corrosion rate. Such point defect based models are developed at the present time for clay environments for deep geological repository [10]. In the future, they could be adapted to concrete environments.

Empirical modelling of the passive corrosion rate will be deduced from experimental programs in progress at CEA and EDF. After 1 year or more exposures to aerated water saturated sound concrete at 20 °C and 50 °C, the carbon steel corrosion measured

by weight loss on different steel specimens did not exceed 0.15 μm/year. As expected, the corrosion rate of steel in sound concrete is very low and more accurate determination of the corrosion rates will be obtained on specimens still being tested under such conditions over longer period of time. Moreover, additional tests are in progress to investigate the steel corrosion behaviour in deaerated concrete. Such an accurate determination of the steel corrosion rate will be a key input data for the oxide layer formation modelling presented in Section 3.2. Indeed, in the case the oxide layer would be composed of siderite, previous calculations show that siderite dissolution kinetic (0.3 μm/year) and steel corrosion rate (~0.15 μm/year) have the same order of magnitude. In that case, concrete cracking may not occur.

Experimentally, angle resolved XPS measurements have been used to analyse steel samples immersed in alkaline solutions (pH 12.4) during several durations [12]. By comparing the deconvolution of the Fe-2p3/2 spectrum obtained at different analysis angles, a schematic representation of the composition of the surface films formed has been proposed. The results indicated that the base layer in contact is composed of FeII and the upper layer is constituted of Fe_2O_3 and FeOOH compounds (see Fig. 5). A similar composition had been proposed by Carnot et al. [13] for a E24 mild steel sample in contact with filtered solution of cement (pH 13). Passive film thicknesses didn't exceed 7 nm even after 8 months immersion. These results confirm that passive films formed on carbon steel in concrete environments are very thin. Unfortunately, such experiments do not give access the corrosion rate since the quantity of corrosion products dissolved in the aqueous solution was not measured. Nevertheless, this shows that depending on diffusion and precipitation processes of corrosion products in concrete, the oxide film formed under passive state conditions may or may not grow in thickness and therefore, lead or not to concrete cracking.

When considering old reinforced concrete samples (aged of 50 years old) [14], passive zones presented corrosion scales that were composed mainly of magnetite (Fe_3O_4) surrounding the metallic core, but some wüstite (FeO) was sometimes present as a dense layer in contact with the metal (Fig. 6). Locally, on the external part of the corrosion layer, hematite (α-Fe_2O_3) was detected. The succession of these three phases from the metallic core to the external zone is characteristic of a high temperature corrosion layout (over 570 °C) [15]. In fact, wüstite can not form at this temperature. Its presence could be due to the hot working of the rebars during their manufacturing. They have then been put in the concrete without any removing of this calamine. Very locally, on few micrometers, goethite could be present at the metal/corrosion products interface. Thicknesses of this typical corrosion layer were between 10 and 50 μm.

4.2. Active corrosion state

4.2.1. Active corrosion kinetics

In aerated chlorinated environments, active corrosion rates have been estimated through laboratory experiments. The objectives of the experimental study were to measure by destructive methods the general corrosion rate (weight loss technique) and the pitting corrosion depth (optical microscope observations) of the samples exposed to various environments [16]. Moreover, an original approach of localised corrosion evaluation has been developed [17]. This empirical model consists in estimating the maximum depth of the localised corrosion as a function of the general corrosion depth. It is based on the pitting factor criterion (P) which can be defined as the ratio between the maximum pit depth (D) and the average general corrosion depth (X) observed at the same time. The pitting factor has been determined for carbon steel under numerous conditions compiled from the literature [17]. When these data are plotted as a function of the average corrosion depth, it can be observed that whatever the experimental conditions, the pitting factor is systematically below an envelope curve, which represents the decrease of the pitting factor with increasing general corrosion depth:

$$P = 4.64X^{-0.67} \quad (X \text{ in mm}).$$

In other words, the localised corrosion rate decreases faster than the general corrosion rate. Then, knowing the general corrosion depth, the maximum pit depth (D) can be deduced from the previous equation:

$$D(\text{mm}) = 4.64X^{0.33}.$$

Such measurements of the maximum pit depth on specimens which have a limited surface may underestimate the theoretical maximum depth because this value depends on the sample area. Although the depth of the deepest pit obeys to the extreme value statistics, some studies have shown that areas of few hundreds of cm^2 are large enough to have a fair estimation of the maximum pit depth [18]. Moreover, this relationship has been determinate on the base of a very large corrosion database including field experience observations measured on multimetric specimens. Data from every specimens of every different size are all consistent with this model.

The maximum pit depth measured on each specimen extracted from the concrete varied from 19 to 264 μm depending on the testing conditions and duration. The evolution of the deduced pitting factor versus the general corrosion depth is presented in Fig. 7. The results were consistent with the empirical model and most of them were one order of magnitude below the envelope curve proposed for the estimation of the maximum pit depth. Moreover, the empirical model has been compared to many others concrete

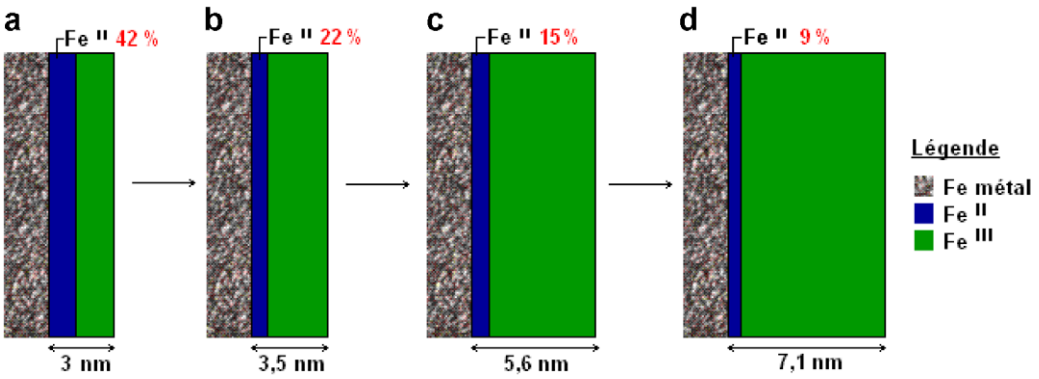

Fig. 5. Schematic representation of the passive film formed on a mild steel immersed in 0.1 M NaOH solution for (a) 1 h, (b) 2 days, (c) 1 month, (d) 8 months.

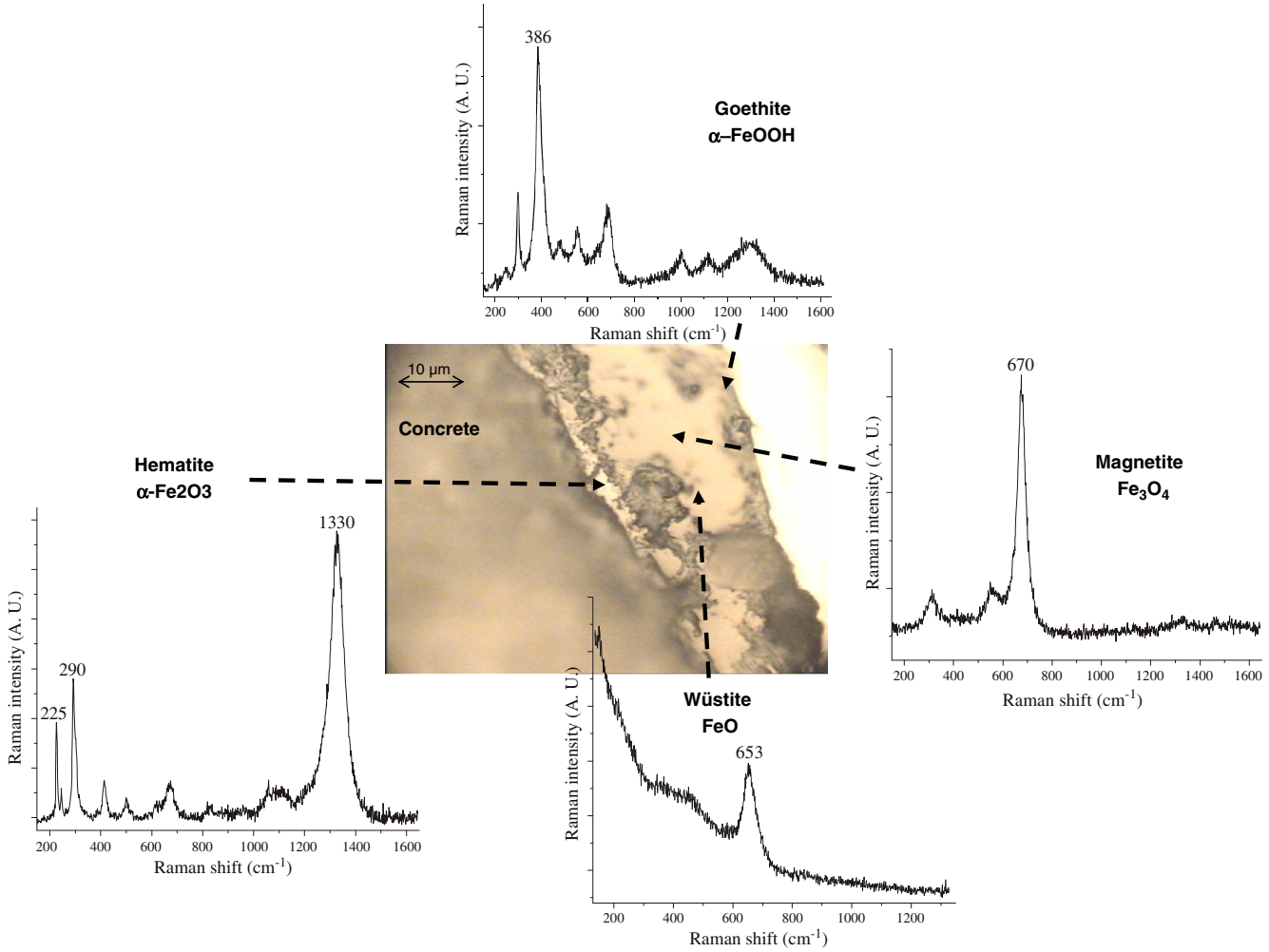

Fig. 6. Microphotograph of a 'passive' corrosion zone and micro-Raman spectra of the different corrosion products [14].

corrosion cases from the field experience coming from EDF internal cases. It gives a good estimation of the maximum pit depth which can be observed under various conditions (carbonated concrete, chloride containing concrete, saturated or not) over long periods of exposure (up to 40 years).

In atmospheric carbonated environments, following characterizations of archaeological analogues, aged from 30 to 650 years, it was possible to evaluate the average corrosion rates [19]. For this purpose, the total iron quantity involved in the corrosion products has been measured by compositional analyses. Then, a density correction allows converting this quantity into metal loss. Results had shown that corrosion rates are around 5 µm/year for all samples.

4.2.2. Corrosion mechanisms in aerated atmospheric conditions

In the case of an active corrosion state, corrosion rate is not limited by the presence of a compact oxide layer but by a porous corrosion products layer. Thus, in the case of reinforced concretes placed under aerated conditions, the oxygen transport through the porous layers (concrete, CPL) and the oxygen reduction are the two main mechanisms that can be limiting steps of the concrete/porous oxide layer/metal system. In this context, localisation of the oxygen reduction at the inner or the outer interface of the porous oxide layer is a key challenge to mechanistically model the long-term corrosion.

Studies performed on ancient systems corroded in hydraulic binders showed that the CPL are mainly formed by a layer of goethite (FeOOH) in which are embedded more or less iron oxides marblings as maghemite or magnetite (see Section 3.1.2, Fig. 3). Most of these phases are not conductive, only magnetite could allow electron conduction from the metallic substrate to reduce oxygen inside the layer. Thus in order to set up a phenomenological model, this point i.e. the location of the cathodic reaction linked to the oxygen reduction has to be enlightened.

Several tests were performed on archaeological analogues presenting thick corrosion layers in order to precisely localise the cathodic reaction of oxygen reduction. Indeed, these analogues, already presenting their CPL were put in water saturated with ^{18}O, an oxygen isotope that is very rare in natural atmosphere ($[^{18}O]/[^{16}O] = 0.02$). After several weeks of corrosion, samples were cut perpendicularly to the corrosion layers. Using the Nuclear Microprobe of the Pierre Süe Laboratory (Nuclear Reaction Analyses [20]), ^{18}O was detected on the transverse section of the CPL. A clear increase of the $^{18}O/^{16}O$ ratio at the metal/oxide interface was evidenced (Fig. 8) [21]. This observation implies that oxygen reduction cathodic reaction is located at the metal/oxide interface. Thus, it is of primary importance to determine the effective diffusion coefficient of gaseous oxygen in the water within the pores of the CPL as a function of the saturation degree of these pores. To sum up, the oxygen transport properties in the CPL are a crucial parameter and have to be determined in addition to the one of the concrete.

4.2.3. Analytical modelling for corrosion rate evaluation

The previous exposed studies allow selecting a main hypothesis of the calculations, that is to say that the cathodic process linked to

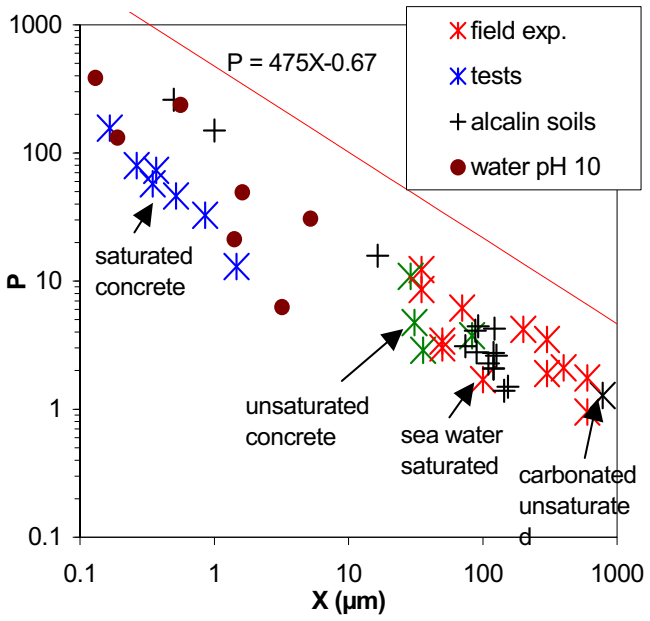

Fig. 7. Evolution of the pitting factor of carbon steels vs. the general corrosion depth [16].

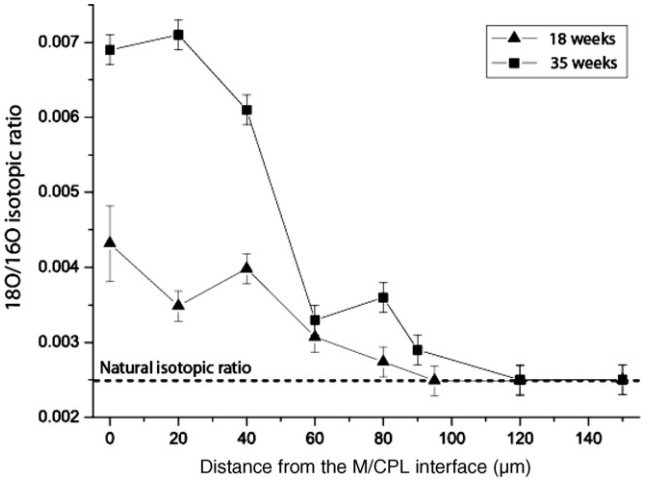

Fig. 8. ^{18}O distribution in the CPL layers after corrosion tests in isotopic medium.

the oxygen behaviour limits the corrosion mechanism. Hypotheses and calculations steps are precisely detailed elsewhere [22]. Studies allow the determination of the global corrosion rate regarding elementary mechanisms (oxygen reduction at the metal/CPL interface, or diffusion of oxygen in the unsaturated concrete, or in the CPL) and considering that goethite is the only corrosion product formed during the corrosion process, as expressed in the following equation:

$$V(t) = \frac{4}{3}\frac{M(\mathrm{Fe})}{\rho(\mathrm{Fe})}\frac{c_{O_2}}{\frac{1}{k\phi S_r} + \frac{\mathrm{th(CPL)}}{D_{e,\mathrm{CPL}}(t)} + \frac{\mathrm{th(TM)}}{D_{e,\mathrm{TM}}(t)} + \frac{\mathrm{th(CC)}}{D_{e,\mathrm{CC}}(t)}},$$

where c_{O_2} is the oxygen concentration available at the steel/concrete interface [mol/m^3], M(Fe) is the iron molar mass (55.8 g/mol), and ρ(Fe) is the iron density (7.8 g/cm^3), th(CC) is the concrete cover thickness [m], th(CPL) is the CPL thickness, th(TM) is the TM thickness [m], ϕ is the oxide layer porosity, measured previously as 10–15% [19], k is the kinetic constant of oxygen reduction (10^{-5} m/s, see [22]), S_r is the water saturation degree of the oxide layer, $D_{e,\mathrm{CPL}}$ and $D_{e,\mathrm{TM}}$ are the diffusion coefficient of oxygen in the Corrosion Product Layer and in the Transformed Medium respectively. $D_{e,\mathrm{CPL}}$ has been measured in diffusion cells under water saturation conditions (RH = 100%) and a value of 2.6×10^{-11} m^2/s was obtained [23].

In order to be able to estimate the corrosion rate of reinforcement in atmospheric conditions, the link between oxygen reduction rate and water content of the concrete has to be modelled. Actually, oxygen diffusion coefficients depend on the water saturation degree of the system: when the relative humidity decreases, the diffusion coefficient increases. These experimental results are usually fitted with a function proposed by Papadakis et al. [24]:

$$D_{e,\mathrm{CC}}(t) = a(1 - \mathrm{RH}(t))^b,$$

with a [m^2/s] and b are the parameters obtained when fitting the experimental curves with Papadakis law. The values of these parameters depend on the water/cement ratio (w/c): a is equal to 1.2×10^{-8} m^2/s for $w/c = 0.4$ and increases with this ratio whereas b decreases while w/c increases. In that condition, the value of the relative humidity (RH) is needed. For this purpose, the saturation degree evolution of the concrete cover was considered by a concrete drying model.

The validity of the drying-corrosion modelling approach was tested through some calculations on a real affected structure. The building is the 55 years old *Chateau d'eau Perret*, of CEA Saclay centre, France (Fig. 9(A)). Before its repair in 2004, degradations such as spalling have been recorded. They occurred mainly on some of the vertical columns supporting the tank, located on the side of the tower exposed to winds. On these columns, two representative damaged zones have been selected for the simulation: one zone at the outer corner of the column (zone 1), and the other (zone 2) close to the junction of the column with the wall (Fig. 9(B)).

Before the repair works, a sampling campaign has been carried out. Concrete and steels have been sampled in the selected zones. The corrosion pattern has been assessed with optical microscope, XRD and μRaman spectroscopy. These characterizations allowed to know the nature of iron oxides constituting the corrosion product layer (mainly goethite α-FeOOH). SEM-EDS studies allowed to determine the thicknesses of the corrosion products layer and of the transformed medium. Considering the nature of the phases present in the different zones and their densities, it was possible to evaluate the quantity of iron involved in the corrosion pattern, and so the average corrosion rate.

Considering an initial concrete water saturation level of 0.95, the water saturation level estimated around the rebars after 55 years is around 0.55 (Fig. 10(A)). It can be noticed that neither seasonal variations of relative humidity of the atmosphere nor rain events have been considered in these calculations. Consideration of these aspects in the simulation will constitute one of the main challenges for the future works.

Drying-corrosion calculations provided a 240 μm equivalent iron thickness after 55 years of corrosion (Fig. 10(B)). Metal losses measured on site were in a range of 20–300 μm. Calculations are coherent with the most important thicknesses characterized on reinforcements.

5. Mechanical consequences of rebars corrosion

The mechanical consequences of corrosions are (i) the reduction of the resistive section of reinforcements (ii) the creation of expansive products (commonly denoted rust) (iii) the steel embrittlement due to pitting corrosion and finally (iv) the cracking of concrete. Programmes developed at CEA and EDF are dedicated to these aspects [25–27]. The following paragraph will focus on

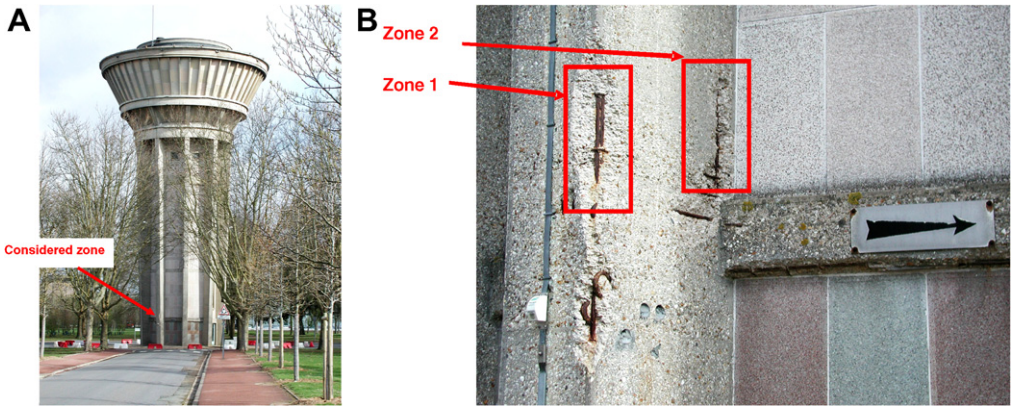

Fig. 9. (A) Photograph of the water tower 'Perret', CEA Saclay centre, France; (B) zoom on a column presenting cracks and spalling of concrete.

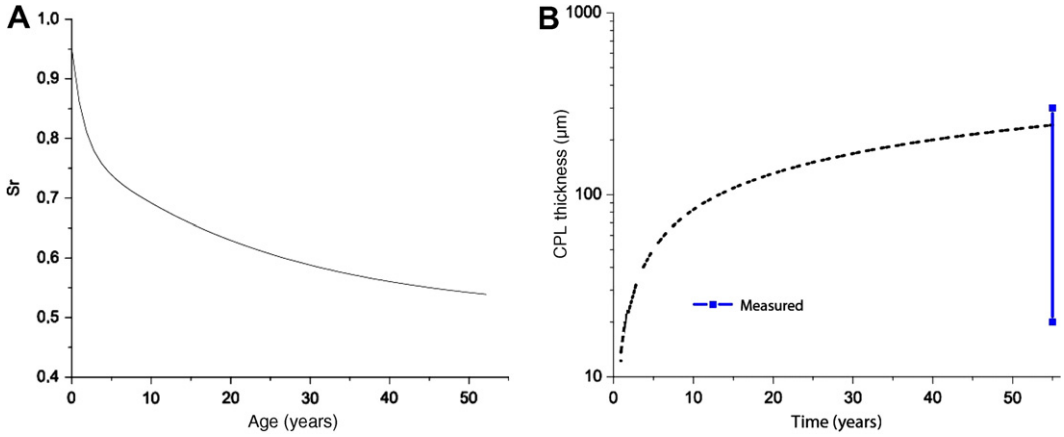

Fig. 10. (A) Evolution with time of the concrete saturation degree at a 4 cm depth (drying model); (B) evolution with time of the CPL thickness (corrosion model) compared with the measurements after 55 years.

the modelling approach developed to predict the concrete cracking due to rebars corrosion.

For this purpose, a damage model has been developed (CORDOBA model [28,29]). This modelling mimics, at a macroscopic scale, the multi-layers structure of the corrosion pattern, by assigning different material behaviour laws to the concrete (concrete and transformed medium), the reinforcements (metallic substrate) and the interface (corrosion product layer).

The development of the corrosion products is simulated by means of special interface finite elements which are placed between the rebars and the concrete, and which can swell with time. One difficulty in this model lies in the determination of the interface parameters in terms of stiffness (Young's modulus for example) and swelling to reproduce the development of corrosion. Since the interface elements are composed of two superposed surfaces (or lines in a bidimensional case), their thicknesses must be

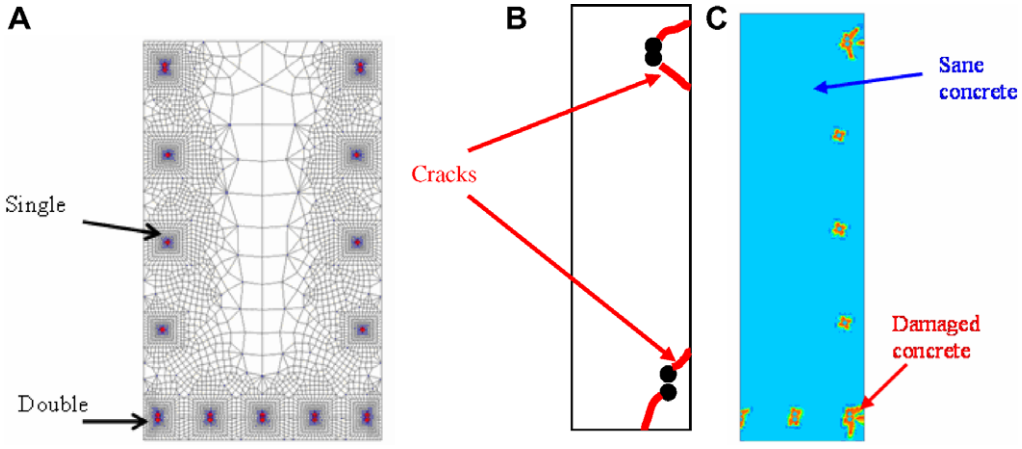

Fig. 11. (A) Mesh of a transverse cross-section of the column; (B) scheme of the observed cracking pattern; (C) predicted cracking pattern.

given through their equivalent stiffnesses, k_n the normal one and k_t the shear one which are proportional to the Young's modulus of the rust (E).

The two stiffnesses are then calculated as following:

$$k_n = \frac{E}{\mathrm{th(CPL)}} \quad \text{and} \quad k_t = \frac{E}{2(1+\nu)} \times \mathrm{th(CPL)},$$

where ν is the Poisson's ratio of the rust, and th(CPL) is the thickness of the CPL, calculated as the product of the expansion rate by the time. The expansion rate depends itself on the average corrosion rate as well as on the volumetric expansion of the corrosion products [30]. The computations are performed using the CEA finite elements code CAST3M [31].

As for the corrosion model, the chosen building is the 55 years old *Chateau d'eau Perret*, of Saclay, France. Applying a corrosion induced cracking model to such an historical building is not a straightforward exercise. Indeed, much information related to the initial state of the structure is not known. In the present case, it has not been possible to find maps and drawings presenting the real positions and diameters of the rebars. A mesh has been established after Ferroscan analyses (Fig. 11(A)).

Despite all limits of input data for the CORDOBA model, the observed cracks at the front or at the rear of the column after 50 years are well predicted, as shown on Fig. 11(B) and (C). In this sense, the CORDOBA model is validated in term of cracking pattern prediction.

6. Conclusions

This paper presents a specific approach that is developed in France at CEA and EDF for the prediction of long-term behaviour of structures involved in the context of the nuclear waste management (cell structures and some types of containers). These programmes deal with interactive modelling studies to predict the corrosion of reinforcing steels and mechanical behaviour of objects for several hundred years, short term in-lab experimentations (corrosion and mechanical behaviour of structures), and finally validate some hypotheses with analyses of corrosion systems on multi secular periods (ancient ferrous artefacts).

Concerning the chlorinated environments, the critical chloride threshold for steel depassivation has been identified. Moreover, an empiric modelling has been proposed to estimate the maximum depth of the localised corrosion as a function of the general corrosion depth. It has been showed that whatever the experimental conditions, the pitting factor is systematically below an envelope curve which represents the decrease of the pitting factor with increasing general corrosion depth.

As far as atmospheric carbonated environments are concerned, results obtained allow the proposition of a mechanistic approach for the long-term corrosion/cracking behaviour of reinforced concrete structures. Characterizations, as well as thermodynamic and kinetic calculations have enabled the identification of the parameters that have to be taken into account.

Finally, a case study has been considered to apply the drying-corrosion-mechanical modelling (Building aged of 55 years) and allow to validate globally the approach and to define future works:

- Experimental work will be conducted to characterize the oxygen transport properties inside the corrosion products layer, the transformed medium and the concrete depending on their water saturation degree. Mechanical properties of these media will also be measured, as well as their hydric behaviour (water permeability, porosity, etc.).
- An experimental program dedicated to deaerated conditions will also be defined to determine the corrosion rate, corrosion products nature and dissolution/precipitation process under such conditions.
- Modelling will be improved by adding a 'chemical' component to the approach, to simulate the carbonation front ingress in the concrete cover. The formation of the transformed medium will also have to be taken into account by the modelling.

All these prospects will allow proposing a coupled carbonation/corrosion/cracking model for long-term behaviour of reinforced concrete structures under both aerated and deaerated conditions that could be used for the nuclear waste management.

References

[1] M. Pourbaix, Atlas of Electrochemical Equilibria in Aqueous Solution, Pergamon, Brussel, 1966.
[2] K. Tuutti, Corrosion of Steel in Concrete, Swedish Cement and Concrete Research Institute, Stockholm, 1982.
[3] C. Andrade, C. Alonso, F.J. Molina, Mater. Struct. 26 (1993) 453.
[4] I. Petre-Lazar, Evaluation du comportement en service des ouvrages en béton armé soumis à la corrosion des aciers, PhD thesis, Université de Laval, Québec, 2000.
[5] A. Pourbaix, V. L'Hostis, in: Proceedings of the NUCPERF 2006 Workshop, Cadarache, France, 27–30 March 2006, J. Phys. IV 136 (2006) 71.
[6] B. Huet, V. L'Hostis, F. Miserque, H. Idrissi, Electrochim. Acta 51 (1) (2005) 172.
[7] F. Miserque, B. Huet, D. Bendjaballah, G. Azou, V. L'Hostis, in: Proceedings of the NUCPERF 2006 Workshop, Cadarache, France, 27–30 March 2006, J. Phys. IV 136 (2006) 89.
[8] J. Van der Lee, CHESS tutorial and cookbook, Technical report LHM/RD/99/05, ENSMP, France, 1999, <http://www.cig.ensmp.fr/~vanderlee/chess/download/tutorial-2.4.pdf>.
[9] V. Neff et al., Corros. Sci. 48 (2006) 2947.
[10] C. Bataillon, in: International Workshop Prediction of Long Term Corrosion Behaviour in Nuclear Waste Systems, Cadarache, 26–29 November 2001.
[11] D.D. MacDonald, J. Electrochem. Soc. 139 (1992) 3434.
[12] F. Miserque, B. Huet, D. Bendjaballah, G. Azou, V. L'Hostis, H. Idrissi, in: Proceedings of the Eurocorr 2005 Conference, Lisbonne, Portugal, 4–8 September 2005, ISBN 972-95921-2-8.
[13] A. Carnot, I. Frateur, S. Zanna, B. Tribollet, I. Dubois-Brugger, P. Marcus, Corros. Sci. 45 (2003) 2513.
[14] V. L'Hostis, D. Neff, L. Bellot-Gurlet, P. Dillmann, Mater. Corros, in press.
[15] J. Philibert, A. Vignes, Y. Brechet, P. Combrade, Métallurgie du minerai au matériau, Masson, Paris, 1998.
[16] F. Foct, I. Petre-Lazar, in: Proceedings of the Eurocorr 2004 Conference, 2004.
[17] F. Foct, J.-M. Gras, in: International Workshop 'Prediction of long term corrosion behaviour in nuclear waste systems', Cadarache, France, 26–29 November 2001, EFC Series 36, 2002.
[18] D. Najjar, M. Bigerelle, C. Lefebvre, A. Iost, ISIJ Int. 43 (5) (2003) 720.
[19] W.J. Chitty, P. Dillmann, V. L'Hostis, C. Lombard, Corros. Sci. 47 (6) (2005) 1555.
[20] E. Vega, P. Berger, P. Dillmann, Nucl. Instrum. and Meth. B 240 (2005) 554.
[21] W.-J. Chitty, P. Berger, P. Dillmann, V. L'Hostis, Corros. Sci., in press.
[22] B. Huet, V. L'Hostis, G. Santarini, D. Féron, H. Idrissi, Corros. Sci. 49 (2007) 1918.
[23] W.J. Chitty, P. Berger, P. Dillmann, V. L'Hostis, G. Béranger, in: Proceedings of the NUCPERF 2006 Workshop, Cadarache, France, 27–30 March 2006, J. Phys. IV 136 (2006) 295.
[24] V.G. Papadakis, C.G. Vayenas, M.N. Fardis, ACI Mater. J. 88 (4) (1991) 363.
[25] V. L'Hostis, C. Brunet, O. Poupard, I. Petre-Lazar, in: Proceedings of the NUCPERF 2006 Workshop, Cadarache, France, 27–30 March 2006, J. Phys. IV 136 (2006) 273.
[26] O. Poupard, V. L'Hostis, S. Catinaud, I. Petre-Lazar, Cement Concrete Res. 36 (2006) 504.
[27] A. Ouglova, Y. Berthaud, F. Foct, M. François, F. Ragueneau, I. Petre-Lazar, Mater. Struct. 41 (2008) 969.
[28] A. Millard, V. L'Hostis, R. Faquin, in: Proceedings of the Conference FRAMCOS (Fracture Mechanics of Concrete and Concrete Structures), Catania (Italie), 17–22 June 2007.
[29] Q.T. Nguyen, S. Caré, A. Millard, Y. Berthaud, Compte Rendus Mécanique 335 (2007) 99.
[30] Y. Liu, RE. Weyers, ACI Mater. J. 95 (6) (1998) 675.
[31] P. Verpeaux, A. Millard, T. Charras, A. Combescure, in: Proceedings of the SMIRT Conference, Los Angeles, USA, 1989.